# Supercritical CO2 assisted foam extrusion for aeronautical sandwich structure manufacturing

Evangelos Dimos, Raffaele D'elia, Martial Sauceau, Romain Sescousse, Luis Enrique Quiroga Cortes, L. Sanches, Guilhem Michon

# SUPERCRITICAL $CO_2$ ASSISTED FOAM EXTRUSION FOR AERONAUTICAL SANDWICH STRUCTURE MANUFACTURING

*Evangelos DIMOS[a], Raffaele D'ELIA[a*], Martial SAUCEAU[b], Romain SESCOUSSE[b], Luis QUIROGA CORTES[a], Leonardo SANCHES[c] and Guilhem MICHON[c]*

a: IRT Saint-Exupéry, 3 rue Tarfaya – CS34436 – 31405 Toulouse Cedex 4, France
b: Centre RAPSODEE, IMT Mines Albi, CNRS, Université de Toulouse – 81013 Albi, France
c: Université de Toulouse, ISAE, ICA, CNRS, 3 rue Caroline Aigle – 31400 Toulouse, France

* corresponding author (raffaele.delia@irt-saintexupery.com)

**Abstract:** *Sandwich structures represent a very interesting approach for the development of new multifunctional and lightweight materials for aerospace and space applications. Nomex® or aluminum honeycomb is at this date the most widely used core materials for sandwich structures, given their extraordinary strength-to-weight-ratio. However, these materials exhibit some important drawbacks as a poor vibrational and acoustic damping [1], along with a limited impact energy absorption capability. Several studies are in progress in order to develop new composite materials with enhanced acoustic and vibrational damping properties [2-8]. A very promising solution to overcome these issues is represented by thermoplastic foams, having several advantages as ease of processing, good impact energy absorption, recyclability and enhanced properties in terms of thermal and acoustic isolation [9-12], along with the possibility to modify their intrinsic properties through micro and nano-particles addition.*

*A relatively new and promising technique to develop thermoplastic foams is represented by supercritical $CO_2$ (sc-$CO_2$) assisted foam extrusion [13,14], with sc-$CO_2$ acting as Physical Blowing Agent (PBA). Sc-$CO_2$ has limited environmental impact, given its low toxicity and energetic requirements to attain its supercritical conditions (31 C, 74 bars), making this process economic, sustainable and totally green. In the frame of this work, a continuous process has been used to produce PLA foams with different microstructures depending on the operating conditions. Typical densities range from 20 to 60 kg/m$^3$, crystallinity from 10 to 30 % and cell size from 90 to 500 µm.*

**Keywords:** Supercritical $CO_2$, PLA polymer, extrusion foaming, sandwich structures, aeronautical materials

## 1. Introduction

Classic sandwich structures are widely used in several industrial sectors but have significant shortcomings such as low damping and sound insulation rates [1], as well as low impact resistance. In aeronautical structures, noise can have significant effects on the health of passengers and aircrew [15] and several studies are in progress with the aim of developing new solutions with enhanced sound insulation [2-6, 16]. Through its potentially nonlinear viscoelastic properties, the intrinsic damping of the core material influences the amplitude of the vibration and acoustic response of the structure. Thus, the study of the vibro-acoustic behavior of the core material is fundamental.

  doi:10.5075/epfl-298799_978-2-9701614-0-0  

A promising solution is to use cellular core materials such as thermoplastic polymer foams. Poly lactic acid (PLA) is a biopolymer that has been extensively studied in recent years, due to its promising potential in reducing waste by replacing petroleum-based polymers. Indeed, PLA monomers can be derived from renewable sources such as corn starch [17,18]. Furthermore, PLA has been considered as a non-toxic/eco-friendly polymer, with a good combination of mechanical properties and ease of processing. This family of materials has in fact several advantages, such as ease of implementation, the ability to absorb energy during an impact (resilience), recyclability and increased properties in terms of thermal and acoustic insulation [19,22]. Moreover, their intrinsic properties can be easily optimized by the dispersion of nano or micro particles.

In this context, the development of alveolar composites shows significant scientific and industrial interest. A certain number of technologies allow the realization of alveolar structures, most conventional using physical blowing agents (PBA) and chemical blowing agents (CBA) which are incorporated into the molten polymer. The gas formed in situ by chemical reaction (CBA) or injected into the polymer (PBA) will create pores or cells and will thus generate porosity in the polymer. However, the use of these compounds poses several problems: (i) CBAs, which are generally carbonated salts that decompose into gases under the action of heat, leave residues in the polymer after formation of the porous network and their decomposition often requires high temperatures; (ii) PBAs, such as freons (CFCs, HCFCs, etc.), are harmful to the environment by attacking the ozone layer or, like hydrocarbons such as pentane or butane, pose safety issues due to their flammability.

Supercritical fluid technology, and more particularly supercritical $CO_2$ (sc-$CO_2$), could respond to these problems by offering an alternative free of the aforementioned defects [14]. It is widely described in the literature and, in recent years, has been extensively studied with biopolymers in order to manufacture "green" foams with a clean process. The process has also been applied to technical thermoplastics such as polyphenylene sulphide and polyamide [23-26], but only with batch foaming processes which involve long implementation times, in particular for the saturation of the polymer by the fluid under pressure. It is possible to overcome these very long saturation times and thus increase the production rate by carrying out the polymer-supercritical fluid mixture continuously in an extruder [27-30]. In this continuous process, the polymer is melted, then sc-$CO_2$ is injected and the mixing actions of the extrusion screw allow to obtain a single-phase mixture. Nucleation then takes place at the injection point. However, the injection process remains a semi-discontinuous process and it seems relevant to think about a totally continuous implementation to reach the highest production rates.

The purpose of the study concentrated in the manufacturing of polymer foams and tested their properties in order to come to a stage that could be integrated in aeronautical structures. At a first stage, an extrusion foaming process of PLA polymer was examined at different operating conditions. Samples with a range of porosity were managed to be fabricated.

## 2. Materials and methods

### 2.1. Materials

The basic raw materials used in this study are PLE 005-A from NaturePlast supplied in the form of granules and a sc-$CO_2$ fluid used as physical blowing agent.

  doi:10.5075/epfl-298799_978-2-9701614-0-0  

### 2.2. Extrusion foaming process

Experiments of extrusion foaming are performed on a single-screw extruder, described in details in previous publications [14]. A schematic representation of the equipment is shown in Figure 1. The single-screw extruder has a 30 mm screw diameter and a length-to-diameter ratio (L/D) of 37 (Rheoscam, Scamex). PLA is inserted into the hopper, while the screw drives the transportation of the solid granulated polymer to the end of the extruder where a die is placed. Along the way towards the exit, the polymer is melted and subsequently mixed with sc-$CO_2$. The foaming process of the polymer takes place when it flows out from a homemade die.

The extruder is thermo-regulated at six locations: $T_1$ and $T_2$ before the $CO_2$ injection port, $T_3$ and $T_4$ after the injection port, $T_5$ in the static mixer and $T_6$ at the die. There are three temperature and four pressure sensors: $P_1$ after the $CO_2$ injector, $P_2$ and $T_{mat1}$ before the second gastight ring, $P_3$ and $T_{mat2}$ before the static mixer and $P_4$ and $T_{mat3}$ close to the die.

The sc-$CO_2$ is injected into the extruder using a syringe pump (260D, ISCO) between the second and the third temperature control device at the same pressure as that of the polymer ($P_1$). The screw rotation speed is kept constant at 30 rpm during the whole experiment and a constant volume flow rate of sc-$CO_2$ ($Q_{CO2}$) is used. Temperatures $T_1$ to $T_4$ are kept constant, while $T_5$ and $T_6$ are progressively decreased while keeping them equal. Samples are collected once a steady state is established [27-30].

The mass fraction of $CO_2$ $\omega_{CO2}$ in the $CO_2$-polymer mixture is calculated as follows:

$$\omega_{CO2} = \frac{Q_{CO2}\rho_{CO2}^{pump}}{Q_{CO2}\rho_{CO2}+\dot{m}_p} \quad (1)$$

$\dot{m}_p$ is the mass flow rate of the polymer measured by weighing outside of the die and $\rho_{CO2}^{pump}$ is the density of $CO_2$, in the pump. This density is obtained from NIST website [31].

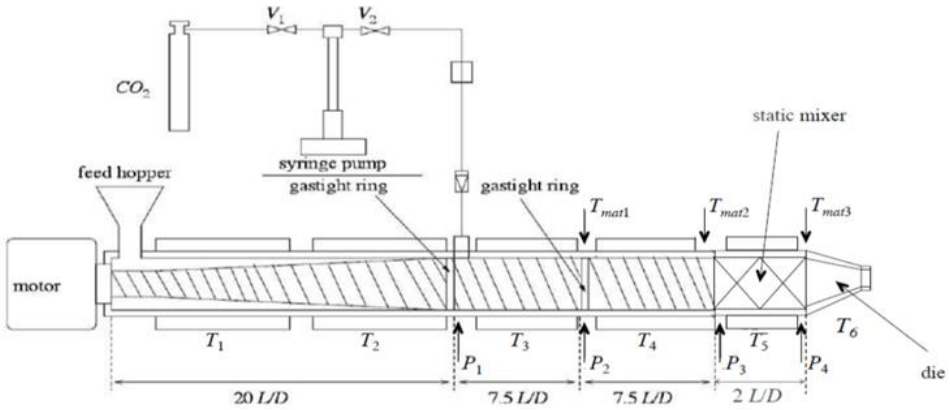


*Figure 1. The experimental system used [25].*

### 2.3. Influence of operating conditions on porosity

The supercritical $CO_2$ assisted extrusion process has shown that the expansion rate or the type of porosity were dependent on temperature. Indeed, with a die temperature too high, a loss of $CO_2$ is present which limits the expansion of the foam. Decreasing the temperature of the die, the surface of the foam is more quickly solidified and retains $CO_2$. Moreover, with the decrease in temperature, the diffusion of gas at the surface of the polymer decreases and therefore more gas remains in the foam to contribute to its expansion. However, an excessive die temperature

  doi:10.5075/epfl-298799_978-2-9701614-0-0 published under CC BY-NC 4.0 license 

decrease penalizes the expansion, the surface of the extruded sample becoming too rigid and therefore limiting expansion. In the case of a semi-crystalline polymer, this surface stiffening is often related to crystallization. Furthermore, it was observed that the temperature upstream of the die also had an influence while it reduces the coalescence of cells thanks to an increase in the melt strength. The $CO_2$ content also plays a key role. With decreasing temperature, the viscosity polymer increases which can lead to pressure increases within the extruder. Adding more $CO_2$ in the extruder plasticizes the polymer and therefore reduces viscosity and pressure, which allows working at lower temperatures [14].

### 2.4. Foam characterization

Porosity ($\varepsilon_{sample}$) is defined as the ratio of void volume to total volume and is calculated as follows:

$$\varepsilon_{sample} = \frac{v_{porosity}}{v_{Total}} = 1 - \frac{\rho_m^{H_2O}}{\rho_P^{H_2O}} \quad (2)$$

$\rho_m^{H_2O}$, is the apparent density of the foamed sample determined by water pycnometry, while $\rho_P^{H_2O}$ is the density of the solid polymer determined on a sample after extrusion by water pycnometry.

The samples obtained by extrusion foaming process are characterized by Scanning Electron Microscopy (SEM) in order to define the cells microstructure and diameter. Cells diameters (*di*) and surfaces ($S_i$) are measured using ImajeJ open source software for image analysis. The average cell size of the foamed samples is calculated according to the following equation:

$$d_{sample} = \sum_{i=1}^{n} \frac{S_i d_i}{S_i} \quad (3)$$

Sample crystallinity of the extruded foams is measured using Differential Scanning Calorimetry (DSC), applying a constant heating rate of 10 °C/min from 20 to 200°C to samples obtained directly after the extrusion. For each grade of material five samples of 10-15 mg were tested using sealed aluminum pans. The defined thermal cycle allows evaluating the cold crystallization enthalpy ($\Delta H_c$) and the enthalpy of fusion ($\Delta H_m$). These parameters are necessary to compute the degree of crystallinity ($X_c$) of the PLA foam, determined according to Equation (4) [13, 14]:

$$X_c = \frac{\Delta H_m - \Delta H_c}{\Delta H_\infty} \quad (4)$$

Where $\Delta H_\infty$ is the theoretical enthalpy of fusion of the material equal to 93 J/g [14].

## 3. Results and discussion

### 3.1. Porosity of PLA foamed samples

Five samples were taken at the extruder outlet and are listed in table 1. This table indicates the temperature $T_{5\text{-}6}$ of the static mixer and die, the pressure $P_4$ before the die, the mass fraction of $CO_2$ $\omega_{CO2}$, porosity $\varepsilon_{sample}$, density $\rho_m^{H_2O}$, diameter $d_{sample}$ and crystallinity $X_c$.

Figure 2 represents the pressure before the die $P_4$, and the final material porosity $\rho_m^{H_2O}$, both measured as a function of the final temperature $T_{5\text{-}6}$. The two variables follow a similar tendency,

  doi:10.5075/epfl-298799_978-2-9701614-0-0 published under CC BY-NC 4.0 license 

inversely proportional to temperature. Indeed, when the temperature decreases, an increase of the porosity can be observed. This increase is small as the porosity level is already high. The pressure also increases due to the increase of the polymer viscosity, despite the plasticizing effect of the increasing mass fraction of the $CO_2$.

*Table 1: Overview of PLA foamed samples.*

| N° | $T_{5\text{-}6}$ (°C) | $P_4$ (bar) | $\omega_{CO2}$ (%) | $\varepsilon_{sample}$ (%) | $\rho_{sample}$ (g/cm³) | $d_{sample}$ (µm) | $X_c$ (%) |
|---|---|---|---|---|---|---|---|
| 1 | 110 | 122 | 2.5 | 97.5 | 0,037 | 500 | 7 |
| 2 | 105 | 135 | 3 | 97.6 | 0,032 | 380 | 14 |
| 3 | 100 | 137 | 3.5 | 97.6 | 0,029 | 290 | 12 |
| 4 | 95 | 145 | 4 | 97.9 | 0,025 | 220 | 23 |
| 5 | 90 | 160 | 4.5 | 98.1 | 0,023 | 140 | 24 |

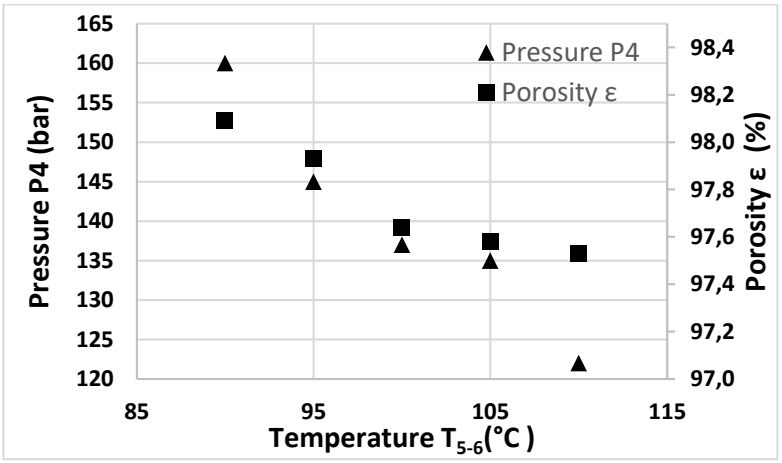


*Figure 2. Behavior of porosity in temperature and pressure*

### 3.2. Scanning electron microscope SEM

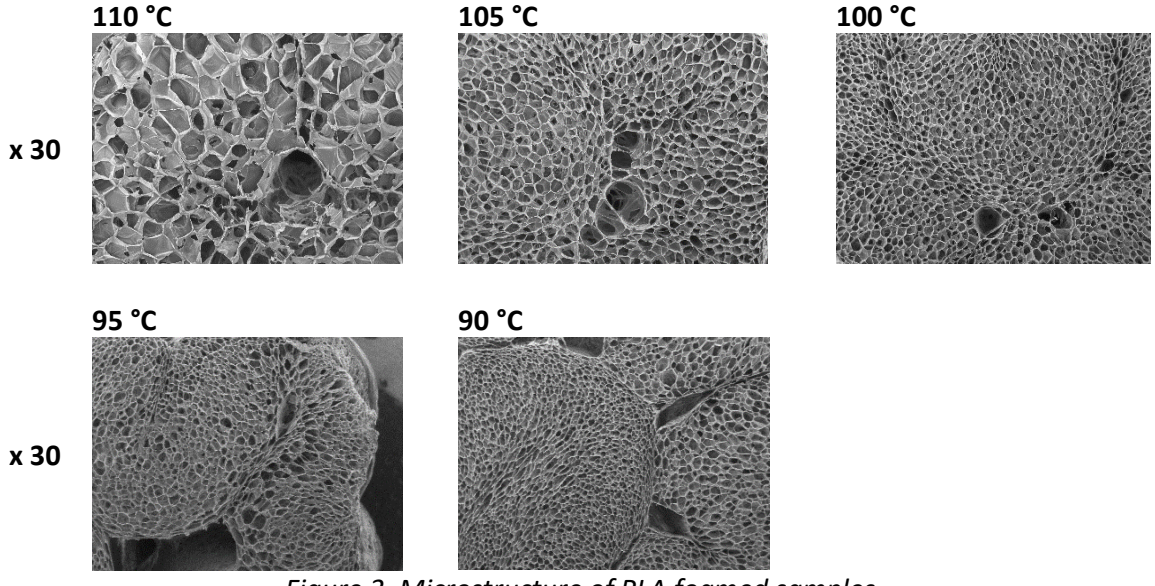


*Figure 3. Microstructure of PLA foamed samples*

  

The SEM photomicrographs of the different foams are shown in Figure 3. The images indicate the influence of temperature on the size and number of cells. The first image shows that, at high die temperature, few pores are present, they are very large and the structure is very coarse. All the other images represent that the pores are smaller at lower temperatures. In addition, the pore walls are slightly torn, confirming that the porosity is closed at the same time. The big cell in the middle is due to the annular shape of the die. The average cell diameters are presented in Table 1 (equation 3). It confirms that the mean diameter decreases with the temperature from 500 µm at 110°C to 140 µm at 90°C. This variation with temperature is obtained at a high level of total porosity which is more or less constant and it shows that it is possible to tune the porous structure by means of the temperature.

### 3.3. Crystallization properties of PLA foamed samples

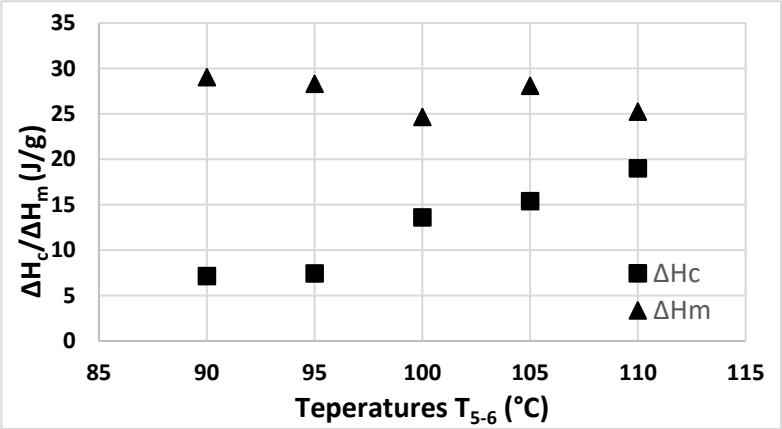


*Figure 3. Behavior of crystallinity with temperature*

After completing a first heating cycle for all five samples, the crystallinity of the samples was calculated using equation 4. The results are summarized in Table 1 and plotted in Figure 3, where the evolution with temperature of the two enthalpies is presented: the melting enthalpy ($\Delta H_m$) and the cold crystallization enthalpy ($\Delta H_c$). It has to be noticed that the crystallinity $X_c$ is proportional to the difference between these two enthalpies. As the die temperature decreases, the melting enthalpy seems to slightly increase, while a more important evolution is observed for the cold crystallization, which decreases. It results in an increase of the sample crystallinity with decreasing temperature, the sample at the lower temperature (90 °C) having a crystallization degree of 24 %, while the sample at the higher temperature (110 °C) presenting a level of only 7 %.

A possible explanation arises from the viscosity of the polymer, which increases with the temperature decrease. Indeed, this viscosity increase provokes a decrease of the Reynold number (the flowrate being more or less constant) and thus the obtention of a more laminar flow inside the die. This flow evolution is favorable to the organization of the polymer chains and thus to the increase of the degree of crystallinity of the final material.

## 4. Conclusions

PLA polymer was the principal material used in this study for the foam's fabrication by continuous extrusion foaming. A series of characterization techniques were implemented including water pycnometry in order to determine the apparent density, scanning electron microscopy to reveal the inner structure of cells and differential scanning calorimetric to

  doi:10.5075/epfl-298799_978-2-9701614-0-0  

measure the crystallization properties of the foam. All these parameters are strongly influenced by the processing temperature and thus to CO2 mass fraction which has to be increased to reach the lower temperatures. Finally, it is possible to tune the cellular structure of the foam at a high level of porosity (97-98 %) by means of the operating temperatures: a more crystalline porous structure (24 %) with a smaller cell mean diameter (140 µm) can be obtained while a more amorphous one (7 %) with higher cell mean diameter (400 µm) is obtained at higher temperatures. These materials will be further investigated in the following, in order to integrate them in composite sandwich structures and a full study of the acoustic and damping mechanical properties is planned.

## 5. Acknowledgement

The authors would like to thank the STAE Foundation (Science & Technologies pour l'Aeronautique & l'Espace) for their financial contribution in the ONOMATOPE project (élabOration de NOuvelles Mousses AéronauTiques avec Optimisation des Performances Elasto-plastiques).

## 6. References

1. Petrone G, D'Alessandro V, Franco F, De Rosa S, Numerical and experimental investigations on the acoustic power radiated by aluminium foam sandwich panels, Compos. Struct. 118 (2014) 170–177.
2. Li Z. Vibrational and acoustical properties of sandwich composite materials. Ph.D. Thesis, Auburn University; 2006.
3. Sargianis, Suhr. Effect of core thickness on noise and vibration mitigation in sandwich composites. Compos Sci Technol 2012; 72:724–30.
4. Liang JZ. Prediction of sound transmission losses for polymer/inorganic particle composites. Polym. Compos. 2015: 36: 2059–2065.
5. Liang JZ, Jiang XH. Sound proofing effect of polypropylene / inorganic particle composites. Compos. B. Eng. 2012; 43: 1995–1998.
6. Zhao HG, Liu YZ, Wen JH, et al. Dynamics and sound attenuation in viscoelastic polymer containing hollow glass microspheres. J. Appl. Phys. 2007; 101: 123.
7. Piolleta, E., Poquillon, D., Michon, G., Dynamic hysteresis modelling of entangled cross-linked fibres in shear, Journal of Sound and Vibration, 383, 248-264, 2016.
8. Quiroga Cortes, L., Sanches, L., Bessaguet, C., Chevalier, M., Lacabanne, C., Dantras, E., G. Michon. Improving damping capabilities of composites structures by electroactive films containing piezoelectric and conductive fillers, Smart Materials and Structures 2021, vol. 30 (8), 085008.
9. Hanssen AG, Girard Y, Olovsson L, Berstad T, Langseth M. A numerical model for bird strike of aluminium foam-based sandwich panels. Int J Impact Eng 2006; 32:1127–44.
10. Hou S, Li Q, Long S, Yang X, Li W. Crashworthiness design for foam filled thinwalled structures. Mater Des 2009; 30:2024–32.
11. Mills NJ, Fitzgerald C, Gilchrist A, Verdejo R. Polymer foams for personal protection: cushions, shoes and helmets. Compos Sci Technol 2003; 63:2389–400.
12. Reglero JA, Rodríguez-Pérez MA, Solórzano E, de Saja JA. Aluminium foams as a filler for leading edges: Improvements in the mechanical behaviour under bird strike impact tests. Mater Des 2011; 32:907–10.
13. Chauvet M, Sauceau M, Fages J. Extrusion assisted by supercritical CO2: a review on its application to biopolymers. J. Supercrit. Fluids, 2017, 120, 408-420.

  doi:10.5075/epfl-298799_978-2-9701614-0-0 published under CC BY-NC 4.0 license 

14. Chauvet M. Extrusion assistée par CO2 supercritique appliquée au moussage d'un biopolymère, le poly (acide lactique), seul ou en mélange à de l'amidon : étude expérimentale et modélisation. 2017. Doctorat de l'Université de Toulouse.
15. Mellert V, Baumann I, Freese N, Weber R, Impact of sound and vibration on health, travel comfort and performance of flight attendants and pilots, Aerosp. Sci. Technol. 12 (1) (2008) 18–25.
16. Sargianis J, Suhr J. Core material effect on wave number and vibrational damp- 99 ing characteristics in carbon fiber sandwich composites, Compos. Sci. Technol. 100 72 (13) (2012) 1493–1499.
17. Murariu M, Dubois P. PLA composites: from production to properties. Adv Drug Deliv Rev 2016; 107:17–46.
18. Lasprilla AJ, Martinez GA, Lunelli BH, Jardini AL, Maciel Filho R. Poly-lactic acid synthesis for application in biomedical devices—a review. Biotechnol Adv 2012;30 (1):321–8.
19. Hanssen AG, Girard Y, Olovsson L, Berstad T, Langseth M. A numerical model for bird strike of aluminium foam-based sandwich panels. Int J Impact Eng 2006; 32:1127–44.
20. Hou S, Li Q, Long S, Yang X, Li W. Crashworthiness design for foam filled thinwalled structures. Mater Des 2009; 30:2024–32.
21. Mills NJ, Fitzgerald C, Gilchrist A, Verdejo R. Polymer foams for personal protection: cushions, shoes and helmets. Compos Sci Technol 2003; 63:2389–400.
22. Reglero JA, Rodríguez-Pérez MA, Solórzano E, de Saja JA. Aluminium foams as a filler for leading edges: Improvements in the mechanical behaviour under bird strike impact tests. Mater Des 2011; 32:907–10.
23. Ma Z, Zhang G, Shi X, Yang Q, Li J, Liu Y, Fan X, Microcellular foaming of poly (phenylene sulfide)/poly (ether sulfones) blends using supercritical carbon dioxide. Journal of Applied Polymer Science 132(40), 2015.
24. Liu WH, Huang YM. Carbon Dioxide-Blown Expanded Polyamide Bead Foams with Bimodal Cell Structure. Ind. Eng. Chem. Res., 2019, 58, 2958-2969.
25. Xu M, Yan H, He Q, Wan C, Liu T, Zhao L, Park CB. Chain extension of polyamide 6 using multifunctional chain extenders and reactive extrusion for melt foaming. Eur. Polym. J., 2017, 96, 210-220.
26. Royer JR, Siripurapu S, Henon FE, Genzer J. Processing of polyamide 11 with supercritical carbon dioxide. Ind. Eng. Chem. Res., 2001, 40, 5570-5577.
27. Villamil Jiménez J A, Le Moigne N, Bénézet J C, Sauceau M, Sescousse R, Fages J. Foaming of PLA Composites by Supercritical Fluid-Assisted Processes: A Review. *Molecules* 2020, *25*, 3408.
28. Le Moigne N, Sauceau M, Benyakhlef M, Jemai R, Benezet J C, Rodier E, Lopez-Cuesta J M, Fages F. Foaming of poly(3-hydroxybutyrate-co-3-hydroxyvalerate)/ organo-clays nano-biocomposites by a continuous supercritical CO2 assisted extrusion process. European Polymer Journal, Elsevier, 2014, 61, pp.157-171.
29. Le Moigne N, Sauceau M, Chauvet M, Benezet JC, Fages J. Microcellular foaming of (nano)biocomposites by continuous extrusion assisted by supercritical CO2. In: Biomass Extrusion and Reaction Technologies: Principles to Practices and Future Potential., 2018, Ed.
30. Common C, Rodier E, Sauceau M, Fages J. Flow and mixing efficiency characterisation in a CO2-assisted single-screw extrusion process by residence time distribution using Raman spectroscopy. Chem. Eng. Res. Design, 2014, 92, 1210-1218.
31. NIST. Carbon dioxide, NIST Chemistry WebBook. 2016. url: http://webbook.nist.gov/cgi/cbook.cgi?ID=124-38-9 (cf. p. 61, 62).

  doi:10.5075/epfl-298799_978-2-9701614-0-0  